Competitive Photoelectrochemical Methanol and Water Oxidation with Hematite Electrodes

Benjamin Klahr[#], Sixto Gimenez[†*], Omid Zandi[‡], Francisco Fabregat-Santiago,[†] Thomas Hamann[‡*]

[#] Department of Chemistry, Northwestern University, 2145 Sheridan Road Evanston, Illinois 60208

[†]Photovoltaics and Optoelectronic Devices Group, Departament de Física, Universitat Jaume I, 12071 Castelló, Spain

[‡] Department of Chemistry, Michigan State University, 578 S Shaw Lane, East Lansing, MI 48824-1322

*Email: sjulia@fca.uji.es, hamann@chemistry.msu.edu

Abstract

Photocatalytic water and methanol oxidation were studied at thin film hematite electrodes synthesized by Atomic Layer Deposition (ALD). Systematic photoelectrochemical characterization along with O_2 evolution measurements were carried out in order to better understand the mechanisms of both water and methanol oxidation at hematite electrodes. For methanol-water mixtures, water and methanol are oxidized competitively with each other, allowing the detection and assignment of distinct surface states, during methanol and water oxidation. The measurement of different surface states for methanol and water oxidation, along with the absence of measurable surface states in an inert acetonitrile electrolyte, clearly shows that the detected surface states are chemically distinct reaction intermediates of water or methanol oxidation.

Introduction

Solar energy driven hydrogen production has emerged as one of the most promising candidates to eventually supplant fossil fuel combustion as the chemical fuel of the future, primarily because solar energy is an essentially inexhaustible, decentralized and environmentally benign resource.[1] This process can be carried out using a photoelectrochemical cell with semiconductor electrodes immersed in water where the photo-generated electrons and holes are directly used to reduce and oxidize water, respectively.[2] This scheme involves the spatial separation of the generated gases (O_2 and H_2) and consequently the probability of back reactions to form H_2O from the evolved gases is significantly decreased. Among the various semiconductor materials tested as photoanodes, hematite (α-Fe_2O_3) has received a lot of attention due to its combination of sufficiently broad visible light absorption (up to 590 nm), excellent stability under caustic operating conditions and a valence band positioned sufficiently low to oxidize water.[3,4] Some limitations related to the short collection length of minority carriers have been addressed by nanostructuring, encompassing the orthogonalization of light absorption and minority carrier drift-diffusion directions, as well as alloying strategies.[5-9] Despite recent advances in charge separation, charge collection at the electrode surface has been shown to be a limiting reaction in the overall water splitting process.[10]

In order to boost the efficiency of water splitting photoelectrochemical devices, allowing them to become a viable technology, a detailed understanding of the charge transfer dynamics leading to water oxidation is compulsory. Recent studies on Fe_2O_3 have provided interesting insights into the oxidation mechanisms, recognizing the relevance of surface intermediates for water splitting.[11-14] We recently developed a general physical model, which explicitly includes the existence of a surface state at the semiconductor/liquid interface. This model successfully describes the accumulation of holes at the surface of the semiconductor as an intrinsic part of the water oxidation reaction.[15] When an efficient hole scavenger is placed in the solution, such as $[Fe(CN)_6]^{3-/4-}$, this surface state does not participate in the oxidation process and direct valence band hole transfer to the solution is the dominant oxidation mechanism.[16] Note that this interpretation is not generally accepted, with others suggesting hole trapping at the surface is a process in parallel with direct hole transfer to water.[11,17-19]

Methanol (CH_3OH) oxidation in the presence of H_2O is a well-studied process, particularly for its relevance for the development of methanol based fuel cells.[20] Methanol has also attracted considerable attention for fundamental studies oriented to the photocatalytic elimination of organic compounds in polluted water and air.[21] Additionally, it has been widely employed as a sacrificial hole scavenger for TiO_2, its oxidation leading to the formation of highly reducing hydroxymethyl radicals and consequently to current-doubling.[22] These radicals can further decompose or couple into added value compounds by complex reaction mechanisms[23] and subsequent decomposition can take place by a direct or indirect mechanism.[24-26] In addition, methanol has recently been investigated as a model system of wastewater whose oxidation offers an alternative hydrogen source.[27]

The present study aims to further understand the mechanisms of water and methanol photo-induced oxidation on hematite electrode surfaces. Specifically, the role of a surface state in both media will be resolved, and correlated with the relative rates of water and methanol oxidation. Comparison to an inert acetonitrile electrolyte is also presented which allows confirmation of the assignment of surface states.

Experimental

Hematite electrodes (~60 nm thick) were deposited by atomic layer deposition (ALD) and characterized using a previously described procedure.[15] The electrodes were measured in contact with aqueous electrolytes containing a 0.1 M phosphate buffer (pH 6.9) with 0.2 M KCl as supporting electrolyte. This aqueous electrolyte contained varying amounts of methanol (CH_3OH). Electrolytes containing only methanol as the solvent also contained 0.2 M tetrabutylammonium chloride as supporting electrolyte. The anhydrous methanol and anhydrous acetonitrile solutions were prepared and sealed in an electrochemical cell under nitrogen in a glove box to minimize the water content. Experiments were also performed with pH 13.6 (1M KOH) solutions and with different electrodes which all showed the same trends.

Photoelectrochemical and impedance measurements made in aqueous electrolytes were made using a homemade saturated Ag/AgCl reference electrode. Those made in the anhydrous methanol electrolyte were made using a commercial Ag/AgCl electrode (ESA 66-EE009 “no leak”). Both electrodes were calibrated to a saturated

calomel electrode (Koslow Scientic) and tested regularly in a $[Fe(CN)_6]^{3-/4-}$ solution to ensure consistency. A platinum mesh electrode was used as the counter electrode. Unless noted otherwise, measurements were made under 1 sun illumination (AM 1.5, 100 mW cm^{-2}). Cyclic voltammetry (CV) measurements were carried out immediately after the electrode was held at a positive potential (1.6 V vs Ag/AgCl for aqueous electrolytes, 1.8 V vs Ag/AgCl for the methanol electrolyte, and 1.5 V vs Ag/AgCl for acetonitrile electrolyte) and 1 sun illumination for 60 seconds. This is expected to fully oxidize the surface intermediates. Immediately before scanning the CV, the light is turned off and the CV measurement is made in the dark. For the anhydrous acetonitrile electrolyte, a positive potential of 1.6 V vs Ag/AgCl was applied for 2 hours in order to oxidize any trace H_2O in the solution or adsorbed on the electrode surface. Chopped light *J-V* curves were measured at a scan rate of 75 mV/s and the light was chopped every 266 ms. The current was sampled at a rate of 500 Hz. Steady state *J-V* curves were measured at 20 mV/s. In order to deconvolute the chopped light *J-V* curve from potential, constant potential transients were measured after turning the light on (where the anodic current is measured) and turning the light off (where the cathodic current is measured). These transients are labeled the anodic and cathodic transients respectively. The current was sampled at a rate of 1000 Hz. Impedance measurements were measured at different applied biases using a perturbation amplitude of 10 mV. The frequency range was 10 kHz-10 mHz. Data were fit using Zview software (Scribner Associates). The light source was a 450 W Xe arc lamp (Horiba Jobin Yvon). An AM 1.5 solar filter (Sciencetech Inc.) was used to simulate sunlight at 100 mW cm-2 (1 sun). The pH was determined with a Crison Basic 20 pH meter.

Oxygen measurements were made with an Ocean Optics spectrophotometer using a FOSPOR fluorescent patch. The electrode was illuminated at 2 suns to produce more oxygen and increase the signal to noise ratio. The theoretical amount of oxygen produced was calculated by assuming that 4 holes are required to produce 1 molecule of oxygen.

Results

Figure 1(a) shows the current density, *J*, vs. applied voltage, *V*, curves of Fe_2O_3 in contact with electrolytes with varying concentrations of CH_3OH. When CH_3OH is added to H_2O, a slight cathodic shift of the photocurrent onset takes place (see insert of Figure 1a), in agreement with observations made by other researchers.[11] For anhydrous methanol, however, there is a shallow photocurrent onset observed at a similar potential (0.7 V vs Ag/AgCl), followed by a steeper current onset which mimics the shape measured with water oxidation at hematite electrodes. Surprisingly, there was an anodic shift of approximately 300 mV which was needed to sustain a given photocurrent density of 200 μA cm^{-2} compared to water based electrolytes. This result is in contrast to literature results of hematite photoelectrodes in contact with good hole scavengers, such as $[Fe(CN)_6]^{3-,4-}$ and H_2O_2.[28,29]

A fluorescence probe was used to measure the amount of O_2 produced, which can be used to evaluate the faradaic efficiency of H_2O oxidation. The O_2 concentration was measured at an applied potential of 1.4 V vs Ag/AgCl for H_2O and CH_3OH-H_2O mixture electrolytes and 1.6 V vs Ag/AgCl for the CH_3OH electrolyte such that the photocurrents were approximately equal. This potential difference also accounts for the difference in the flat band potential, E_{FB}, between aqueous and methanol based electrolytes, *vide infra*. In the case of the aqueous electrolyte, the faradaic efficiency due to O_2 production is approximately unity as shown in Figure 1(b) and Table 1. As increasing amounts of CH_3OH are added to H_2O, the faradaic efficiency due to O_2 generation decreased where no O_2 generation could be detected in anhydrous CH_3OH. This is expected since the oxidation of CH_3OH should produce formaldehyde or CO_2, not O_2.[26,30,31] Interestingly, a significant amount of O_2 was generated even with large concentrations of CH_3OH. A summary of the amount of O_2 measured for different CH_3OH concentrations at applied potentials of 0.75 and 1.4 V vs Ag/AgCl can be seen in Table 1. Relative rates, v_R, for CH_3OH oxidation compared to water oxidation was calculated by the equation $v_R = \left(\frac{1-FE}{[CH_3OH]}\right)\left(\frac{FE}{[H_2O]}\right)^{-1}$, where *FE* is the faradaic efficiency for O_2 generation, and can also be found in Table 1. Despite an obvious preference for CH_3OH oxidation compared to H_2O oxidation based on the relative rates shown in Table 1, the overall rate (current) is not significantly altered by adding CH_3OH to H_2O as shown in figure 1a. Poor current

onset potentials still exist with CH_3OH in solution, showing that it is not acting as a fast and model hole collector as others have suggested.[11]

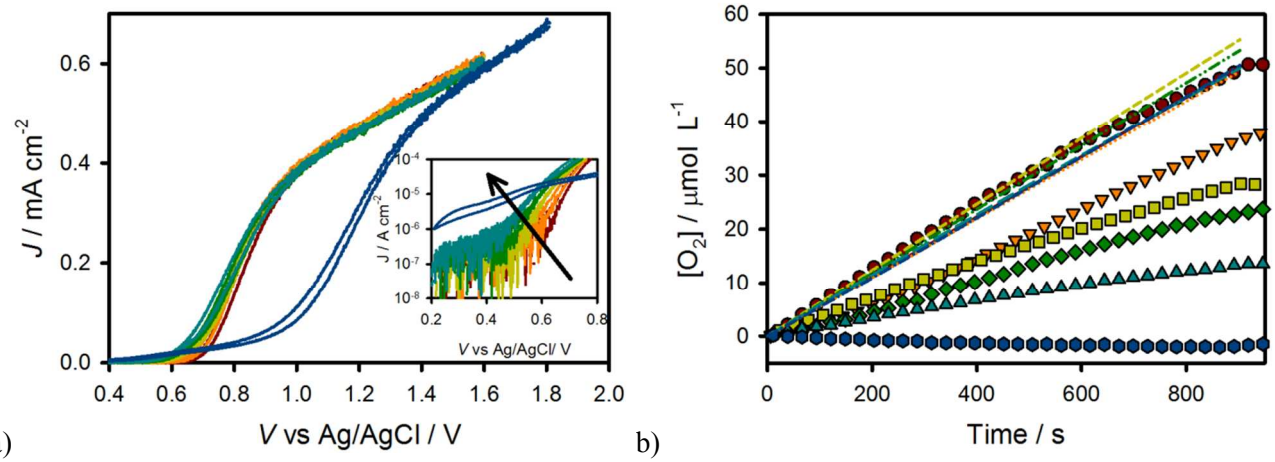

a) b)

Figure 1. a) *J-V* curves of a hematite electrode under 1 sun illumination in contact with H_2O (red), 0.2M CH_3OH (orange), 2M CH_3OH (yellow), 5M CH_3OH (green), 10M CH_3OH (teal), and CH_3OH (blue) vs Ag/AgCl. b) Theoretical oxygen produced under 2 sun illumination (lines) and measured O_2 concentration (shapes) for a hematite electrode in contact with H_2O (solid line and circles), 0.2M CH_3OH (dotted line and downward pointing triangles), 2M CH_3OH (short dashed line and squares), 5M CH_3OH (double dotted dashed line and diamonds), 10M CH_3OH (long dashed line and upward pointing triangles), and CH_3OH (single dotted line and hexagons). Applied potentials for O_2 concentration measurement was 1.4 V vs Ag/AgCl for the H_2O and 5M CH_3OH electrolytes and 1.6 V vs Ag/AgCl for the CH_3OH electrolyte.

Table 1. Summary of faradaic efficiency due to O_2 generation for varying concentrations of CH_3OH in H_2O

		0.75 V vs Ag/AgCl				1.4 V vs Ag/AgCl			
		[O_2] / micromoles L^{-1}				[O_2] / micromoles L^{-1}			
[MeOH] / M	[H_2O] / M	Theoretical	Measured	O_2 Faradaic Efficiency	Relative Rate*	Theoretical	Measured	O_2 Faradaic Efficiency	Relative Rate*
0.0	55.5	11.17	11.11	**99.42%**		50.13	49.81	**99.36%**	
0.2	55.2	7.90	5.41	**68.48%**	133.48	49.20	36.00	**73.17%**	106.33
2.0	50.2	12.90	4.01	**31.09%**	56.52	55.15	28.35	**51.40%**	24.11
5.0	46.7	10.77	1.89	**17.55%**	41.35	53.15	22.80	**42.90%**	11.71
10.0	37.8	7.29	0.59	**8.06%**	37.65	49.86	15.94	**31.97%**	7.02

*Ratio of CH_3OH to H_2O oxidation

In order to account for any differences in energetics (band edge movement) due to the different electrolytes, impedance spectroscopy (IS) measurements were performed in the dark. Mott Schottky plots were generated for pure H_2O, CH_3OH and 5M CH_3OH electrolytes by fitting the impedance spectra to a Randle's circuit. Since the electrode, and therefore dopant density, is the same for all electrolytes, the slope of the Mott Schottky is expected to be independent of the electrolyte. This is indeed the case, apparent from inspection of figure 2a. Therefore, to fit the Mott Schottky plots, the slopes of all 3 electrolytes were fit globally. The extracted dopant density, N_D, was calculated to be 5.3×10^{18} cm^{-3}, in good agreement with previous results.[15,16] The flat band potential was also extracted from the Mott Schottky plots and can be seen in table 2. The measured E_{FB} for the aqueous electrolytes are nearly equal. In anhydrous CH_3OH however, the E_{FB} is shifted ~200 mV positive. Part of the difference in *J-V* curves can therefore be attributed to a shift in the band energies. In order to carry out an adequate comparison between the different electrolytes, potentials were normalized to their respective E_{FB}'s. Normalized *J-V* curves are shown in Figure 2b. At high positive applied potentials, the current achieved in all electrolytes is approximately equal. We have suggested previously that in these thin films, at high applied potential, the photocurrent is controlled by the rate of photogenerated holes that reach the surface; i.e. water oxidation is not the rate limiting step. Thus, addition of a fast hole collector (e.g. H_2O_2, CH_3OH, $Fe(CN)_6^{3-/4-}$) should not increase the current at a given positive Fermi level. Even when correcting for the change in the E_{FB}, the steep current onset of anhydrous CH_3OH oxidation occurs at more positive potentials compared to H_2O oxidation suggesting that photoelectrochemical differences cannot be solely attributed to differences in the position of the bands of Fe_2O_3 in different media.

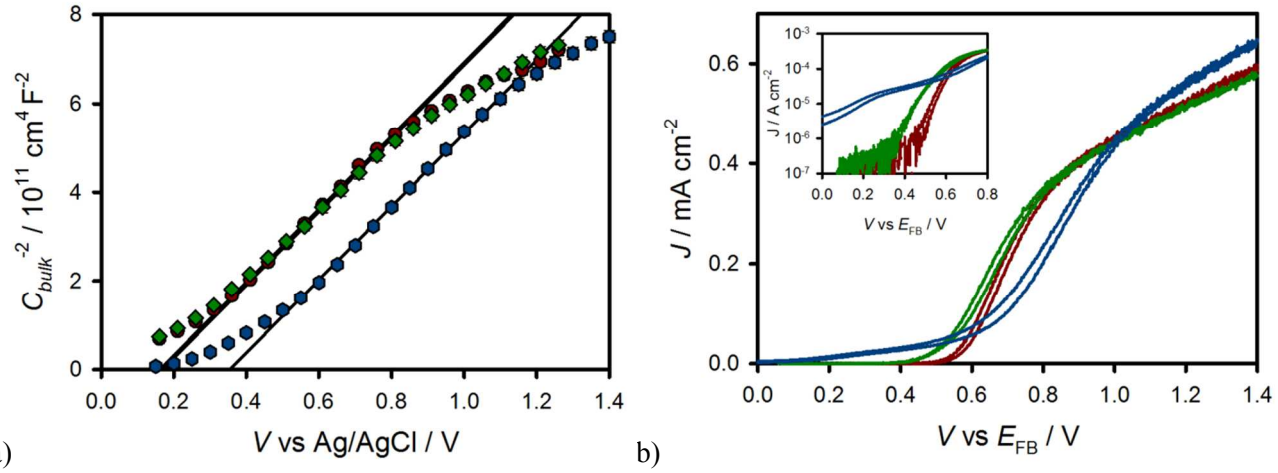

Figure 2. (a) Mott Schottky plot of C_{bulk} measured in the dark for H_2O (red circles), 5M CH_3OH (green diamonds) and CH_3OH electrolytes (blue hexagons). (b) *J-V* curves of a hematite electrode under 1 sun illumination in contact with H_2O (red), 5M CH_3OH (green) and CH_3OH (blue) plotted vs E_{FB}.

Table 2. Summary of the Mott-Schottky analysis from impedance spectroscopy measurements carried out in the dark including the flat band potential (E_{FB}) and the donor density (N_D) of hematite phototoelectrodes in different solution media.

	E_{FB} vs Ag/AgCl (mV)	N_D ($\cdot 10^{18}$ cm^{-3})
H_2O	137	5.3
5M CH_3OH	143	5.3
CH_3OH	330	5.3

In order to get more detailed mechanistic information of water and methanol oxidation, impedance spectroscopy measurements were also performed under illumination conditions. Aqueous electrolytes produced Nyquist plots with two clearly distinguishable semicircles near the current onset potential (supporting info, Figure SI2). A physical model which has been previously developed for the interpretation of charge transfer from hematite electrodes to water can be seen in the form of an equivalent circuit, EC, shown in Figure 2a.[15,16] This general model specifically includes the presence of a surface state able to capture conduction band electrons and valence band holes; the trapping-detrapping kinetics are related to R_{trap}, and the occupancy of the surface state

produces a chemical capacitance, C_{ss}. Charge transfer takes place through this surface state with a charge transfer resistance, $R_{ct,ss}$. Additionally, a bulk capacitance, C_{bulk}, accounts for the space charge capacitance. This EC was used to fit IS data gathered in H_2O and 5M CH_3OH electrolytes. For the pure H_2O electrolyte, a clear peak in C_{ss} develops with voltage which is coincident with the current onset potential (Figure 4a). This peak highlights the requirement for charge accumulation at the surface for water oxidation to occur, and has been pointed out by other researchers.[32-34] When CH_3OH is added to the aqueous solution, a C_{ss} peak is also observed, at the same potential vs E_{FB} as shown in Figure 4(a). The magnitude of this peak is approximately two times lower, however, reflecting that fewer holes are accumulated at the surface in this state. This result is further corroborated by CV measurements presented below. This result is also in good agreement with the O_2 evolution measurements displayed in Figure 1(b), which indicated that both oxidation of water and methanol lead to the obtained photocurrent. A corresponding decrease in C_{ss} and O_2 generation with the addition of CH_3OH further shows that water oxidation occurs through a surface state intermediate. Also, a decrease in the measured C_{ss} for H_2O-CH_3OH mixtures implies that methanol oxidation competes against water oxidation through a different pathway. Despite methanol reducing the measured capacitance of surface states due to water oxidation, two capacitive features are still observed in impedance spectra measured in the anhydrous methanol electrolyte (see Supporting Information, Figure SI 2b). Since it appears that charge transfer to methanol occurs through a different pathway than that of water, we invoke another possible EC to describe anhydrous methanol oxidation at hematite electrodes, which is shown in figure 3b. This model was chosen due to its corroboration with photoelectrochemical experiments discussed below. As in the EC used to describe H_2O oxidation, this EC still contains a surface state capacitance, C_{ss} and a resistance of transfer to those surface states, R_{trap}, based on the observation of 2 clear capacitances in the Nyquist plot. However, instead of charge transfer through those surface sates, this EC contains a separate charge transfer resistance which is not associated with those surface states, R_{ct}. This model could imply direct charge transfer from the valence band of the hematite to methanol through an outer-sphere electron transfer mechanism. However a more likely possibility is that a surface state or surface intermediate is generated, such as a surface adsorbed methoxy species (Fe-O-CH_3) which is the analogous adsorbed species responsible for charge transfer for photogenerated holes on TiO_2.[30] This mechanism could be interpreted as a single charge transfer resistance if the

steady state concentration is very low, resulting in a very low or immeasurable capacitance. By using this model, the obtained trap capacitance shows a double peak feature, with significantly lower intensity compared to water based electrolytes (Figure 4a).

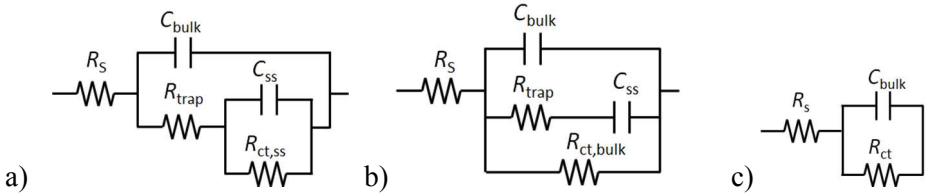

Figure 3. (a) Simplified model involving hole transfer through a surface state (b) Simplified model involving direct hole transfer from valence band (c) Randles circuit

The values of charge transfer resistance R_{ct} are shown in Supporting Information, Figure SI3(a) for the different electrolytes. At low bias (0 - 0.4V vs E_{FB}), the addition of CH_3OH to H_2O reduces the charge transfer resistance. This is because we are measuring the charge transfer resistance from the surface states (due to water oxidation) which is reduced with the addition of CH_3OH, as shown by O_2 evolution measurements and C_{ss}. In other words, for a constant potential, the resistance of charge transfer to water through water oxidation intermediates is reduced because the current due to water oxidation is reduced for an increasing amount of CH_3OH. Compared to aqueous electrolytes, R_{ct} for methanol oxidation is higher, positive of 0.4 V vs E_{FB}, consistent with the lower photocurrents measured at more anodic bias. The values of R_{trap} are compiled in Supporting Information, Figure SI3(b). R_{trap} was found to be identical for both water based electrolytes and higher for anhydrous methanol between 0 V vs E_{FB} and 0.7 V vs E_{FB}. This is likely because hole transfer to CH_3OH is less probable due to the lower C_{ss} and corresponding accepting states.

Confirmation of the fits can be gained by plotting the total resistance from impedance ($R_{tot}=R_s+R_{trap}+R_{ct,ss}$ for aqueous electrolytes and $R_{tot}=R_s+R_{ct,bulk}$ for the CH_3OH electrolyte) and comparing that to the resistance calculated from the *J-V* curves ($R_{tot}=dV/dJ$). This plot can be seen in figure 4b. All electrolytes show R_{tot} from *J-V* curves and R_{tot} from IS are in good general agreement indicating that the main resistances which control the *J-V*

are represented in the impedance spectra. It is interesting to note that anhydrous methanol oxidation involves two different R_{tot} dips, around 0.4 V vs E_{FB} and 0.8 V vs E_{FB}, which appear to be related to the two small C_{ss} peaks shown in Figure 4a. This suggests that two different oxidations are being measured; one between 0.2-0.6 V vs E_{FB} (see Figure 2b) where the slope of the *J-V* curve is low, and one above 0.6 V vs E_{FB}, where the *J-V* curve takes a similar slope as that of aqueous solutions.

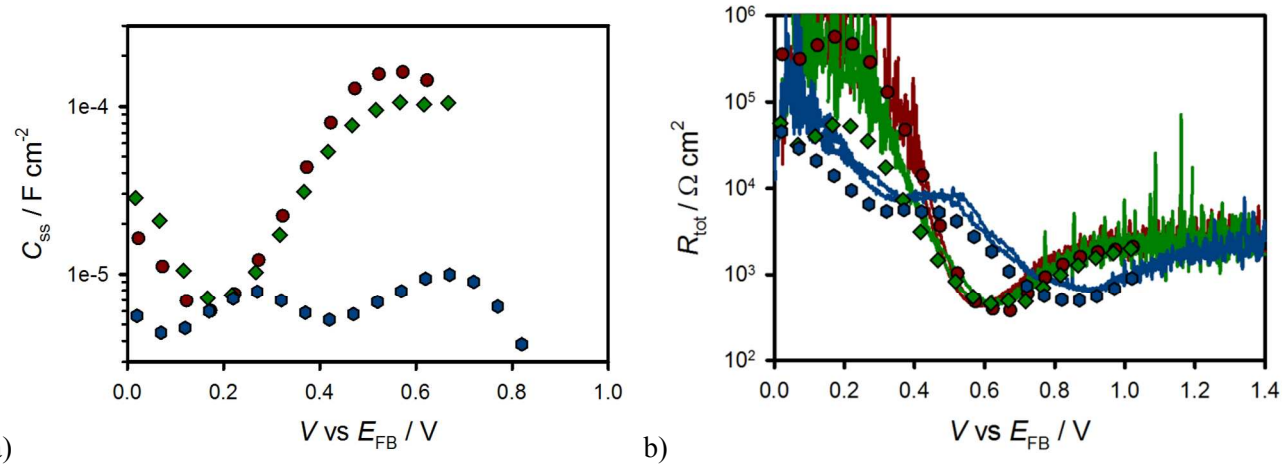

Figure 4. (a) C_{ss} and (b) R_{tot} vs E_{FB} extracted from IS analysis under illumination (100 mW·cm^2) for a hematite electrode in contact with H_2O (red circles) 5M CH_3OH in H_2O (green diamonds) and CH_3OH (blue hexagons).

Cyclic voltammetry experiments were carried out on Fe_2O_3 films to measure surface states as previously reported.[16] For these measurements a constant high positive bias (1.6 V vs Ag/AgCl for aqueous electrolytes and 1.8 V vs Ag/AgCl for methanol electrolyte) was initially applied under illumination to fill the surface states with holes. The light was then turned off and a CV was immediately scanned several times (Supporting information, Figure SI4). Cathodic peaks were observed for all electrolytes on the first scan at potentials similar to the potentials where a C_{ss} is observed from IS measurements (Figure 5). These peaks are observed at the same energy and with similar relative intensity to those observed in the peaks of C_{ss} in Figure 4a. Additional figures including data measured in all CH_3OH electrolytes can be seen in supporting information which show the same trend of decreasing cathodic peak currents with the addition of CH_3OH. On the second scan, these peaks disappear

because the surface states are not re-oxidized on the timescale of this experiment (supporting information, Figure SI4). The evolution of this peak with scan rate (supporting information, Figure SI5) also confirms its capacitive nature.[16] Upon zooming in on the cyclic voltammetry curve for methanol (Figure 5 insert), two small peaks are evident, which is consistent with the C_{ss} measured by IS using the model in figure 3b. It should be noted that these two peaks were not observed in the IS interpretation using the model in figure 3a (See Supporting Information, Figure SI7). Thus these two peaks corroborate the selection of the equivalent circuit for interpreting CH_3OH oxidation at the hematite surface.

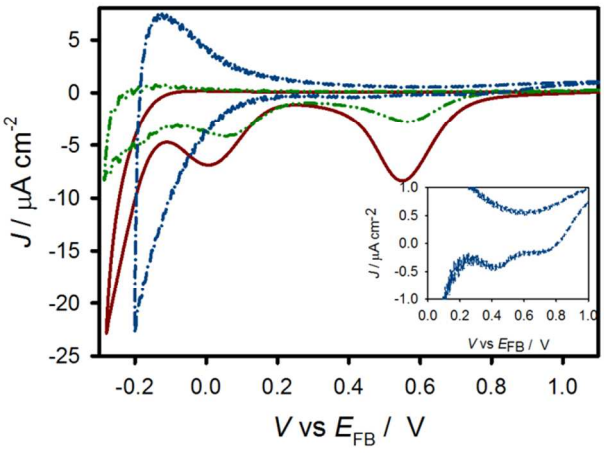

Figure 5. Comparison of the first scan of the CV measured at 200 mV/s in H_2O (red solid line), 5M CH_3OH in H_2O (green double dot dashed line) and CH_3OH (blue single dot dashed line). A magnified image of the CH_3OH curve is shown in the insert which shows 2 small peaks.

The cathodic peak measured at ~0.55V vs E_{FB} in the CVs of Figure 5 along with the C_{ss} peak observed in IS measurements at the same potential, has been previously attributed to the accumulation of photogenerated holes on the hematite surface in the form of water oxidation intermediates. This peak is always coincident with the water oxidation photocurrent onset and its magnitude is correlated to the water oxidation current; i.e. the peak magnitude reduces with increasing CH_3OH concentration which competes for photogenerated holes (less water oxidation intermediates form at a given time) (Figure SI6). To further show that these capacitive features are a part of the oxidation intermediates of water and methanol, analogous CV measurements were performed in an

inert electrolyte, anhydrous acetonitrile, where no hole transfer to solution is expected. The band energy position of the hematite electrode in an acetonitrile electrolyte was controlled through Mott-Schottky measurements, which showed an ~80 mV cathodic shift in the flat band potential compared to aqueous electrolytes (Figure SI8). Illuminated *J-V* curves of a hematite electrode in contact with anhydrous acetonitrile showed negligible background current ensuring the absence of H_2O in the electrolyte (Figure 6a). As shown in Figure 6b for anhydrous acetonitrile solution, no cathodic peaks were observed above the background in the CV measurements suggesting that the cathodic peak observed under H_2O oxidation conditions is specific to H_2O oxidation and not intrinsic to the hematite surface. Interestingly, addition of trace amounts of H_2O to the acetonitrile electrolyte resulted in the development of a cathodic peak in the CV scans, further confirming the assignment of this capacitive feature to species involved in H_2O oxidation reaction (see Supporting Information Figure SI8).

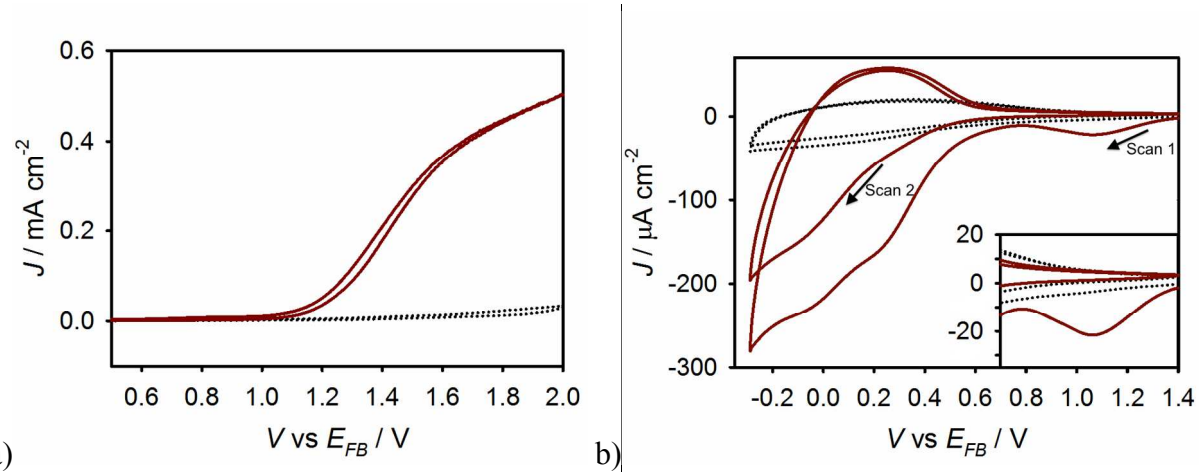

Figure 6. (a) *J-V* and (b) CV response of a hematite electrode measured in contact with anhydrous MeCN (black dotted line) and after addition of 10 µL H_2O (0.2 %V) to the electrolyte (red solid line). *J-V*s were measured under 1 sun illumination and CVs were recorded at 500 mV/s in dark after holding the electrode at 1.5 V vs Ag/AgCl under 1 sun illumination for 60 s.

The capacitive nature of the surface states of both H_2O and CH_3OH surface states was examined by transient light experiments. Chopped light *J-V* curves were obtained and compared to those with constant illumination (Supporting Information, Figure SI9). In all tested electrolytes, the presence of anodic and cathodic transients indicated the presence of surface states.[28,35,36] These spikes were analyzed quantitatively by switching

the light on (anodic) and off (cathodic) at a constant potential while measuring the current as a function of time. Examples of current transients can be seen in Figure 7a and in supporting information, Figures SI10-SI13. Integration of the cathodic current provides a quantitative measurement of the light-induced charge stored in the surface states, which is shown in Figure 7b, and compared to C_{ss} measured by IS. The good agreement between the integrated charge from transient measurements with C_{ss} from IS shows that these two measurements are probing the same species.

Single exponential lifetimes of the cathodic transients were calculated and can be seen in Figure 7c. The lifetimes are approximately equal for H_2O and 5M CH_3OH electrolytes throughout the potential range with the exception of potentials greater than ~0.6 V vs E_{FB} where the mixture has lower lifetimes. These decays are attributed to electrons from the conduction band reducing the oxidized surface states. Since the dominant surface state is related to water oxidation, it is not surprising that these measured lifetimes are constant for the two aqueous electrolytes. We note that this result disagrees with Cowan *et. al.* who showed a decrease in lifetime for a 10% CH_3OH in H_2O solution compared to a H_2O solution under no applied bias.[37] It is possible, however, the techniques of transient electrochemistry employed herein and transient absorption spectroscopy employed by Cowan *et. al.* are measuring different species. In the CH_3OH electrolyte, the lifetimes of these transients are approximately an order of magnitude lower than those measured in aqueous electrolytes at potentials where photocurrent is measured. This is attributed to an increased rate of recombination to surface CH_3OH oxidation intermediates compared to surface H_2O oxidation intermediates.[26] The lifetimes were also calculated by multiplying the C_{ss} and R_{trap} from IS results and are shown in figure 7c as open shapes. The same general trend is observed between the lifetimes calculated from transient and EIS measurements.

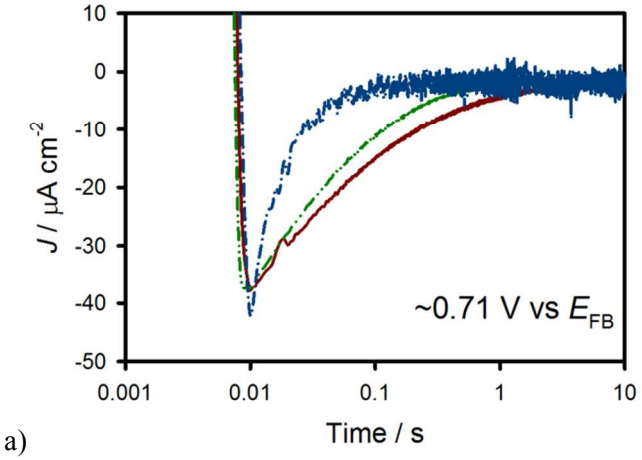

a)

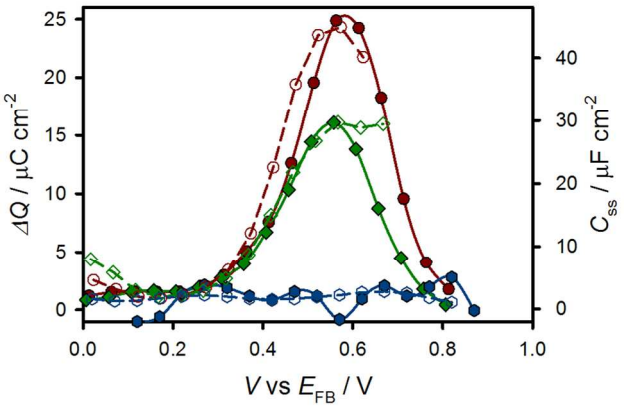

b)

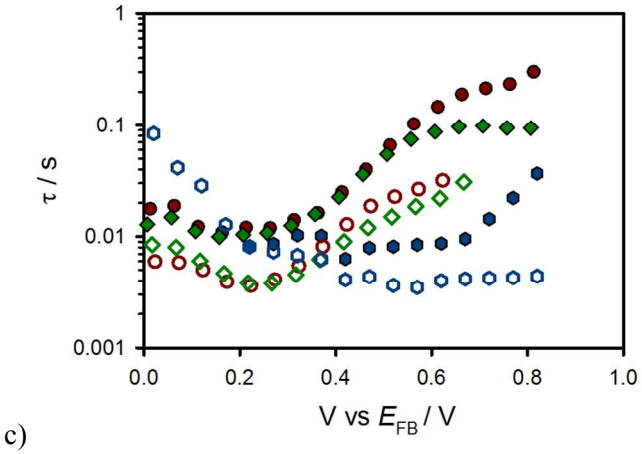

c)

Figure 7. a) Cathodic transients in H_2O (red solid line), 5M CH_3OH in H_2O (green double dot dashed line) and CH_3OH (blue single dot dashed line) measured within 5 mV of 0.71 V vs E_{FB}. b) The calculated charge passed measured by integrating cathodic transients (filled symbols, solid lines) along with C_{ss} measured by IS (hollow symbols, dashed lines) for a hematite electrode in contact with H_2O (red circles) 5M CH_3OH in H_2O (green diamonds) and CH_3OH (blue hexagons). c) Lifetimes of transients fit by a single exponential decay (solid shapes) and by multiplying C_{ss} and R_{trap} (open shapes) for H_2O (red circles), 5M CH_3OH (green diamonds), and CH_3OH (blue hexagons).

From the double peak feature observed for C_{ss} from IS analysis of anhydrous methanol oxidation, correlated to respective cathodic peaks in the cyclic voltammetry, and dips in the charge transfer resistance (R_{ct}) and total resistance (R_{tot}), it appears that two surface intermediates are being measured during CH_3OH oxidation. A recent paper by Baltrusaitis et. al. discusses methanol oxidation on hematite surfaces using theoretical

calculations for several surface terminations.[27] Since the electrochemical response of the oxidation of H_2O-CH_3OH mixtures is dominated by the redox properties of water surface intermediates (which has been previously discussed in detail),[15,16] this discussion will focus on the oxidation of the anhydrous CH_3OH solution. For the Fe-O_3-R termination of the (0001) surface of hematite (which is the most stable termination under non-aqueous conditions),[38] anhydrous methanol oxidation at the Fe atom is expected to occur as follows:[27]

$$CH_3OH + Fe \rightarrow CH_3OFe + H^+ + e^- \quad (1)$$

$$CH_3OFe \rightarrow CH_2OFe + H^+ + e^- \quad (2)$$

$$CH_2OFe \rightarrow CHOFe + H^+ + e^- \quad (3)$$

$$CHOFe \rightarrow COFe + H^+ + e^- \quad (4)$$

Under photoelectrochemical conditions (where U=2.1 eV for photogenerated holes in the valence band), steps 1-4 are calculated to be thermodynamically downhill.[27] While these reactions are thermodynamically favored, insight into the rates cannot be easily determined due to the conflation with electron recombination from electrons in the conduction band to the various surface bound species. The two capacitance peaks observed in IS, and cyclic voltammetry likely represent potentials where a relatively large concentration of surface bound intermediates form due to a balancing of oxidation of holes from the valence band and recombination from electrons in the conduction band. The identity of these two electrochemically observable species is uncertain, although we speculate that each peak is an independent surface species represented in one of equations 1-4. In-situ spectroelectrochemistry has recently been used to examine the identity of water oxidation intermediates at the hematite surface, and could also be employed to study methanol oxidation.[17,39] In this manner, the precise molecular details of this mechanism are currently being investigated in our lab.

Finally, concomitant water oxidation is required to produce O^* and complete the oxidation of CO to CO_2.[27] Since this favored mechanism cannot occur in the anhydrous methanol electrolyte, this explains the very low initial photocurrent densities observed for this electrolyte. Further, in the presence of water, the overall

methanol oxidation cannot proceed faster than the water oxidation reaction required to produce O^*, this explains why the addition of methanol does not have a significant effect on the *J-V* response of methanol-water mixtures: i.e. water oxidation is the rate-limiting step.

Conclusions

The photooxidation of methanol and water was examined at the surface of model hematite photoanodes synthesized by Atomic Layer Deposition (ALD). A surface capacitance correlated with water oxidation is decreased with the addition of CH_3OH. This reduction in surface states, measured by IS, CV and transient measurements, combined with corroborating O_2 evolution, further confirms that the surface states are actively participating in the hole transfer mechanism to H_2O, as suggested in previous studies.[15,16] The fact that distinct surface states are measured in anhydrous methanol solutions, and no surface states are measured in an inert anhydrous acetonitrile solution, further proves this point.

Acknowledgements

TWH thanks the National Science Foundation (CHE-1150378) for support of this research. JB & FFS acknowledge support by projects from Ministerio de Ciencia e Innovación (MICINN) of Spain (Consolider HOPE CSD2007-00007), Generalitat Valenciana (PROMETEO/2009/058 and the "Institute of Nanotechnologies for Clean Energies", under project ISIC/2012/008). FFS thanks the funding of University Jaume I- Bancaixa (Grant P1·1B2011-50).

References

(1) Lewis, N. S.; Crabtree, G. **2005**.
(2) van de Krol, R.; Liang, Y.; Schoonman, J. *Journal of Materials Chemistry* **2008**, *18*, 2311.
(3) Sivula, K.; Le Formal, F.; Graetzel, M. *Chemsuschem* **2011**, *4*, 432.
(4) Lin, Y.; Yuan, G.; Sheehan, S.; Zhou, S.; Wang, D. *Energy & Environmental Science* **2011**, *4*, 4862.
(5) Brillet, J.; Gratzel, M.; Sivula, K. *Nano Letters* **2010**, *10*, 4155.

(6) Lin, Y.; Zhou, S.; Sheehan, S. W.; Wang, D. *Journal of the American Chemical Society* **2011**, *133*, 2398.
(7) Sivula, K.; Zboril, R.; Le Formal, F.; Robert, R.; Weidenkaff, A.; Tucek, J.; Frydrych, J.; Graetzel, M. *Journal of the American Chemical Society* **2011**, *132*, 7436.
(8) Steier, L.; Herraiz-Cardona, I.; Gimenez, S.; Fabregat-Santiago, F.; Bisquert, J.; Tilley, D.; Gratzel, M. *Advanced Functional Materials* **2014**, *DOI: 10.1002/adfm.201402742*.
(9) Zandi, O.; Klahr, B. M.; Hamann, T. W. *Energy & Environmental Science* **2013**, *6*, 634.
(10) Young, K. M. H.; Klahr, B. M.; Zandi, O.; Hamann, T. W. *Catalysis Science & Technology* **2013**, *3*, 1660.
(11) Pendlebury, S. R.; Barroso, M.; Cowan, A. J.; Sivula, K.; Tang, J. W.; Gratzel, M.; Klug, D.; Durrant, J. R. *Chemical Communications* **2011**, *47*, 716.
(12) Pendlebury, S. R.; Cowan, A. J.; Barroso, M.; Sivula, K.; Ye, J.; Gratzel, M.; Klug, D. R.; Tang, J.; Durrant, J. R. *Energy & Environmental Science* **2012**.
(13) Peter, L. M.; Wijayantha, K. G. U.; Tahir, A. A. *Faraday Discussions* **2012**.
(14) Upul Wijayantha, K. G.; Saremi-Yarahmadi, S.; Peter, L. M. *Physical Chemistry Chemical Physics* **2011**, *13*, 5264.
(15) Klahr, B.; Gimenez, S.; Fabregat-Santiago, F.; Hamann, T.; Bisquert, J. *Jounal of the Americal Chemical Society* **2012**, *134*, 4294.
(16) Klahr, B.; Gimenez, S.; Fabregat-Santiago, F.; Bisquert, J.; Hamann, T. *Energy & Environmental Science* **2012**, *5*, 7626.
(17) Barroso, M.; Pendlebury, S. R.; Cowan, A. J.; Durrant, J. R. *Chemical Science* **2013**, *4*, 2724.
(18) Barroso, M.; Cowan, A. J.; Pendlebury, S. R.; Grätzel, M.; Klug, D. R.; Durrant, J. R. *Journal of the American Chemical Society* **2011**, *133*, 14868.
(19) Barroso, M.; Mesa, C. A.; Pendlebury, S. R.; Cowan, A. J.; Hisatomi, T.; Sivula, K.; Grätzel, M.; Klug, D. R.; Durrant, J. R. *Proceedings of the National Academy of Sciences* **2012**, *109*, 15640.
(20) Iwasita, T. *Electrochimica Acta* **2002**, *47*, 3663.
(21) Hoffmann, M. R.; Martin, S. T.; Choi, W.; Bahnemann, D. W. *Chemical Reviews* **1995**, *95*, 69.
(22) Kho, Y. K.; Iwase, A.; Teoh, W. Y.; Madler, L.; Kudo, A.; Amal, R. *Journal of Physical Chemistry C* **2010**, *114*, 2821.
(23) Lu, H.; Zhao, J.; Li, L.; Gong, L.; Zheng, J.; Zhang, L.; Wang, Z.; Zhang, J.; Zhu, Z. *Energy & Environmental Science* **2011**, *4*, 3384.
(24) Chen, J.; Ollis, D. F.; Rulkens, W. H.; Bruning, H. *Water Resources* **1999**, *33*, 669.
(25) Mora-Sero, I.; Villarreal, T. L.; Bisquert, J.; Pitarch, A.; Gomez, R.; Salvador, P. *Journal of Physical Chemistry B* **2005**, *109*, 3371.
(26) Villarreal, T. L.; Gomez, R.; Neumann-Spallart, M.; Alonso-Vante, N.; Salvador, P. *Journal of Physical Chemistry B* **2004**, *108*, 15172.
(27) Baltrusaitis, J.; Hu, Y.-S.; McFarland, E. W.; Hellman, A. *ChemSusChem* **2014**, *7*, 162.
(28) Dotan, H.; Sivula, K.; Gratzel, M.; Rothschild, A.; Warren, S. C. *Energy Environ. Sci.* **2011**, *4*, 958.
(29) Klahr, B. M.; Hamann, T. W. *Journal of Physical Chemistry C* **2011**, *115*, 8393.
(30) Shen, M.; Henderson, M. A. *The Journal of Physical Chemistry Letters* **2011**, *2*, 2707.
(31) Panayotov, D. A.; Burrows, S. P.; Morris, J. R. *The Journal of Physical Chemistry C* **2012**, *116*, 6623.
(32) Cummings, C. Y.; Marken, F.; Peter, L. M.; Tahir, A. A.; Wijayantha, K. G. U. *Chemical Communications* **2012**.
(33) Braun, A.; Sivula, K.; Bora, D. K.; Zhu, J.; Zhang, L.; Graetzel, M.; Guo, J.; Constable, E. C. *Journal of Physical Chemistry C* **2012**, *116*, 16870.
(34) Iandolo, B.; Hellman, A. *Angewamdte Chemie International Edition* **2014**, *126*, 1.
(35) McDonald, K. J.; Choi, K. S. *Chemistry of Materials* **2011**, *23*, 1686.
(36) Le Formal, F.; Tetreault, N.; Cornuz, M.; Moehl, T.; Gratzel, M.; Sivula, K. *Chemical Science* **2011**, *2*, 737.

(37) Cowan, A. J.; Barnett, C. J.; Pendlebury, S. R.; Barroso, M.; Sivula, K.; Grätzel, M.; Durrant, J. R.; Klug, D. R. *Journal of the American Chemical Society* **2011**, *133*, 10134.

(38) Wang, X. G.; Weiss, W.; Shaikhutdinov, S. K.; Ritter, M.; Petersen, M.; Wagner, F.; Schlögl, R.; Scheffler, M. *Physical Review Letters* **1998**, *81*, 1038.

(39) Klahr, B.; Hamann, T. *The Journal of Physical Chemistry C* **2014**, *118*, 10393.